



## Oxidation behavior of porous $\text{Ti}_3\text{SiC}_2$ prepared by reactive synthesis

Hui-bin ZHANG<sup>1,2</sup>, Shu-yu SHEN<sup>1</sup>, Xin-li LIU<sup>2,3</sup>, Zhong-he WANG<sup>2</sup>, Yao JIANG<sup>2</sup>, Yue-hui HE<sup>2</sup>

1. College of Materials Science and Engineering, Zhejiang University of Technology, Hangzhou 310014, China;
2. State Key Laboratory of Powder Metallurgy, Central South University, Changsha 410083, China;
3. School of Materials Science and Engineering, Central South University, Changsha 410083, China

Received 11 May 2017; accepted 30 January 2018

**Abstract:** High-purity porous  $\text{Ti}_3\text{SiC}_2$  with a porosity of 54.3% was prepared by reactive synthesis and its oxidation behavior was evaluated under air in the temperature range from 400 to 1000 °C. Thermogravimetric analysis and differential scanning calorimetry (TG–DSC), scanning electron microscope (SEM), X-ray diffractometry (XRD), energy dispersive spectrometer (EDS), Raman spectrum, BET surface area analysis, and pore-parameter testing were applied to the studies of the oxidation kinetics, phase composition, micro morphology, and porous structure parameters of porous  $\text{Ti}_3\text{SiC}_2$  before and after oxidation. The results showed that the formation of  $\text{TiO}_2$  oxidized products with different modifications was the primary factor influencing the oxidation resistance and structural stability of porous  $\text{Ti}_3\text{SiC}_2$ . Cracks were observed in the samples oxidized in the full temperature range of 400–1000 °C because of the growth stress and thermal stress. At 400–600 °C, anomalous oxidation with higher kinetics and the aberrant decrement in pore size and permeability were attributed to the occurrence of severe cracking caused by the formation of anatase  $\text{TiO}_2$ . At raised temperatures over 600 °C, the cracking phenomena were alleviated by the formation of rutile  $\text{TiO}_2$ , but the outward growth of the oxide scales detrimentally decreased the connectivity of porous  $\text{Ti}_3\text{SiC}_2$ .

**Key words:**  $\text{Ti}_3\text{SiC}_2$ ;  $\text{TiO}_2$ ; porous material; reactive synthesis; oxidation

### 1 Introduction

$\text{Ti}_3\text{SiC}_2$  is a representative material in the family of the layered ternary ceramics called MAX phase materials with the general formula  $\text{M}_{N+1}\text{AX}_N$  ( $N=1, 2$  or  $3$ ), where M is a transition metal, A is an A-group (mostly IIIA and IVA) element, and X is either C or N [1,2]. This material possesses a combination of properties of both metals and ceramics, such as good oxidation resistance, low density (4.52 g/cm<sup>3</sup>), high elastic modulus (~320 GPa) and strength, excellent thermal shock resistance, high damage tolerance and good machinability, and has therefore been generally considered as a new candidate for high-temperature structural materials [3–5].  $\text{Ti}_3\text{SiC}_2$  can be synthesized through various methods (i.e., chemical vapor deposition (CVD), hot pressing (HP), pressureless sintering, spark plasma sintering (SPS) and arc melting) using different starting reactants (i.e.,  $\text{TiH}_2$ , Ti, Si, C, SiC, TiC) [6–10]. Nevertheless, the previous attempts to produce single-phase  $\text{Ti}_3\text{SiC}_2$  bulk samples

usually resulted in the existence of second phases, such as TiC [10–13],  $\text{TiSi}_2$  [10,11,14], and  $\text{Ti}_5\text{Si}_3$  [14]. Accordingly, the oxidation behaviors of bulk  $\text{Ti}_3\text{SiC}_2$  which had been extensively studied were in fact influenced by the presence of impurities. SUN et al [13] investigated the oxidation behaviors of  $\text{Ti}_3\text{SiC}_2$ -based material prepared by in-situ hot pressing/solid–liquid reaction process. They pointed out that the existence of TiC was deleterious to the oxidation resistance of  $\text{Ti}_3\text{SiC}_2$ . RADHAKRISHNAN et al [14] investigated the oxidation behaviors of polycrystalline  $\text{Ti}_3\text{SiC}_2$  which contains 2%  $\text{TiSi}_2$  (volume fraction) at 1000 °C in air for 50 h, indicating that the oxidation of  $\text{Ti}_3\text{SiC}_2$  obeyed a linear law at 1000 °C. TONG et al [15] studied the oxidation of  $\text{Ti}_3\text{SiC}_2/\text{SiC}$  composite at 1000 °C in flowing air for 10 h. They revealed that the presence of SiC had a beneficial effect on oxidation resistance of  $\text{Ti}_3\text{SiC}_2$ . In addition of the second phases, porosity was another key fact that affects the oxidation resistance of bulk polycrystalline  $\text{Ti}_3\text{SiC}_2$ . However, most investigations on the oxidation behavior of  $\text{Ti}_3\text{SiC}_2$  have

been carried out in bulk form up to now [16–19]. Although BARSOUM and EL-RAGHY [20] showed that partly dense samples had a higher oxidation rate, oxidation data of porous  $\text{Ti}_3\text{SiC}_2$  seem rather scarce.

It is well known that porous materials are of high specific surface area, low density, good permeability and brilliant impact energy absorption capacity [21]. Through uniting of porous structure and intrinsic material performance, porous  $\text{Ti}_3\text{SiC}_2$  is exceptionally expected to be applied as functional materials, such as catalytic carriers and filters [11,22]. However, due to the existence of connected open pore which provides the inward transport channel for the oxidizing gas, porous material appears to be susceptible to rapid oxidation, if a continuous oxide scale which physically serves as a barrier between the remaining substrate and the ambient atmosphere over the surface of the porous skeleton cannot be built. To our knowledge, oxidation can cause not only the degradation of mechanical properties but also the failure of permeable porous structure. Obviously, oxidation behavior of porous  $\text{Ti}_3\text{SiC}_2$  should differ from that of dense samples, so it is urgent to be investigated.

In the present study, the oxidation behaviors of porous  $\text{Ti}_3\text{SiC}_2$  with high purity were investigated in the temperature range from 400 to 1000 °C in air. The oxidation kinetics, phase compositions and pore structures after oxidation at different temperatures were systematically characterized. The oxidation resistance and pore-structure stability of porous  $\text{Ti}_3\text{SiC}_2$  were extensively evaluated. Some unique phenomena appearing in the oxidation of porous  $\text{Ti}_3\text{SiC}_2$  were shown.

## 2 Experimental

The synthesis of porous  $\text{Ti}_3\text{SiC}_2$  started with commercial  $\text{TiH}_2$  (CAS No.7704-98-5, purity 99.5%, median diameter 38.3  $\mu\text{m}$ ), Si (CAS No.7440-21-3, purity 99.5%, median diameter 14.6  $\mu\text{m}$ ) and graphite (CAS No.7782-42-5, purity 99.0%, median diameter 5.5  $\mu\text{m}$ ) powders. The above powders were mixed according to a Ti/Si/C molar ratio of 3:1.2:2. No pore-forming agent was added. Excessive silicon addition could make up for the evaporation loss of Si at high temperature during vacuum sintering, which benefited the achieving of single phase  $\text{Ti}_3\text{SiC}_2$  [8]. The powders were gently ball-mixed for 12 h to obtain the homogeneous mixture. The mixture was then compacted into a disk with a diameter of 30 mm under a uniaxial pressure of 200 MPa. To obtain the porous  $\text{Ti}_3\text{SiC}_2$  materials, these green compacts were heated based on designed sintering schedules, and finally sintered at 1350 °C for 3 h in vacuum ( $1.0 \times 10^{-3}$  Pa).

Before oxidation experiments, the average overall

and open porosities of the prepared samples were measured to be 54.3% and 48.6%, respectively, according to the Archimedes method. The measurement of the maximum pore size was based on the bubble point method by recording the minimum pressure necessary to blow through a liquid-filled porous membrane [23]. The gas permeability of porous  $\text{Ti}_3\text{SiC}_2$  was determined on a porous material test instrument (pore structure performance tester, FBP-IV, Northwest Institute for Non-ferrous Metal Research, China). Accordingly, the maximum pore size of porous  $\text{Ti}_3\text{SiC}_2$  samples was measured to be  $\sim 13.2$   $\mu\text{m}$  for average, and gas permeability was  $98.5$   $\text{m}^3/(\text{kPa} \cdot \text{h} \cdot \text{m}^2)$ . The magnified section scanning electron microscopy (SEM, FEI Nano 230) image of the synthesized material is shown in Fig. 1(a). Note that porous  $\text{Ti}_3\text{SiC}_2$  comprised two kinds of pores which had different average pore sizes. It is supposed that the relatively large pores ( $>10$   $\mu\text{m}$ ) were the interstitial pores left from the cold-press and the subsequent sintering processes, while the relatively small pores (3–4  $\mu\text{m}$ ) were generated from reactive synthesis. X-ray diffractometric analysis (XRD, Dmax 2500 VB, Cu  $K_\alpha$ ) showed that no Bragg peaks from the common impurity phases were detected in the resultants (see Fig. 1(b)). The synthesized samples were nearly single-phase  $\text{Ti}_3\text{SiC}_2$  (JCPDS No. 74-0310). From the XRD patterns, the purity of  $\text{Ti}_3\text{SiC}_2$  calculated using the calibrated standard addition method [24] was 99.4%.

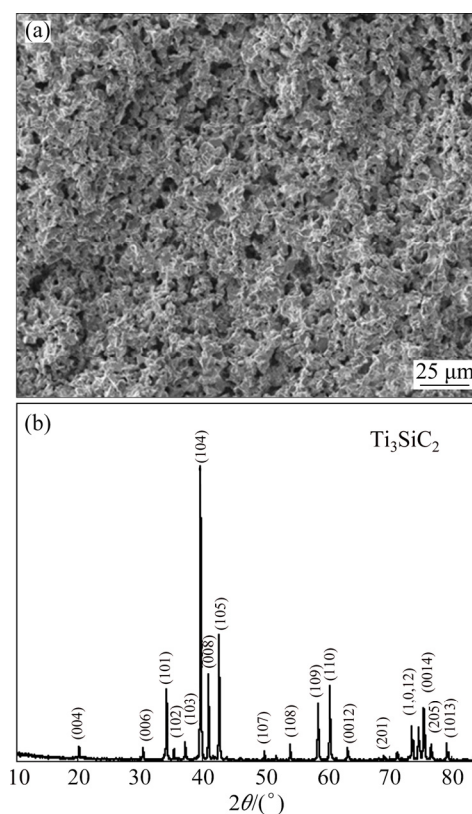


Fig. 1 SEM image (a) and XRD pattern (b) of porous  $\text{Ti}_3\text{SiC}_2$

TG–DSC analysis of porous  $\text{Ti}_3\text{SiC}_2$  was carried out with an instrument (Netzsch STA449C) in the temperature range from ambient temperature to 800 °C in an air flow with a heating rate of 5 °C/min. Afterwards, isothermal oxidation tests were conducted to analyze the oxidation behavior of porous  $\text{Ti}_3\text{SiC}_2$  in air at designated temperatures of 400, 500, 600, 700, 800, 900 and 1000 °C, respectively. The thermogravimetry measurements were performed on an analytical balance with a resolution of 0.1 mg. The measurements of the mass gains and pore parameters were conducted after each oxidation cycle. Phase composition of the samples after oxidation was identified using XRD and Raman spectroscopy (LabRAM HR800, excitation at 488.0 nm using an  $\text{Ar}^+$  laser). The magnified morphology was observed through SEM equipped with an energy-dispersive spectroscopy (EDS). The specific surface areas of the samples were determined by Brunauer–Emmett–Teller (BET) method with an ASAP 2010 volumetric analyzer.

### 3 Results

#### 3.1 Simultaneous TG–DSC and oxidation kinetics

Simultaneous TG–DSC measurements of porous  $\text{Ti}_3\text{SiC}_2$  were carried out in the air flow, as shown in Fig. 2. As can be seen from Fig. 2(a), the TG test showed an appreciable mass increase starting at about 400 °C; from the DTG curve, an anomalous peak of mass gain could be observed at about 600 °C. The DSC curve shown in Fig. 2(b) exhibited three broad overlapped exothermic peaks at temperatures of 400–800 °C, namely peaks I, II and III. The exothermic peak II appeared at 550–700 °C compared favorably with the peak shown in DTG curve. Accordingly, the exothermic peak II could be conceivably attributed to the anomalous oxidation with higher oxidation rate. The other two broad exothermic peaks centered at around 550 °C (peak I) and 700 °C (peak III) were newly discovered in the present study about porous  $\text{Ti}_3\text{SiC}_2$  samples and were further investigated in the following sections.

To understand the oxidation kinetics, isothermal oxidation of porous  $\text{Ti}_3\text{SiC}_2$  was implemented at temperatures of 400–1000 °C for a testing period of 100 h in air. The mass gains were plotted as a function of time as shown in Fig. 3. Visual inspection showed that the mass gain curves did not follow a single law and that all isotherms could be divided into two stages, i.e., the early stage with a fast oxidation rate and the late stage with a slow oxidation rate. The mass increments of the samples initially varied from 2.4% to 47.7% with increasing the oxidation temperature, but at time more than 30 h the oxidation processes performed at

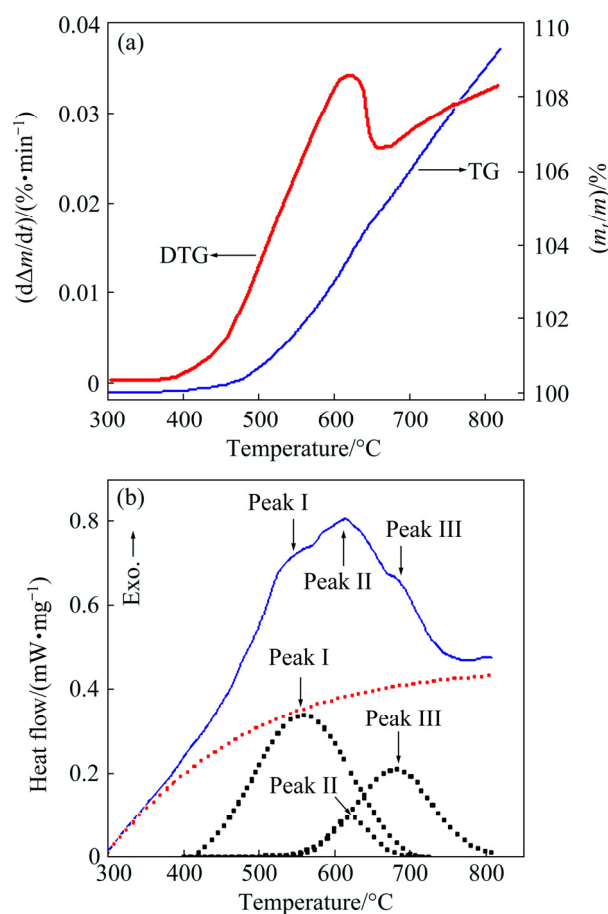


Fig. 2 TG–DTG (a) and DSC (b) curves of porous  $\text{Ti}_3\text{SiC}_2$  at heating rate of 5 °C/min in dry air flow

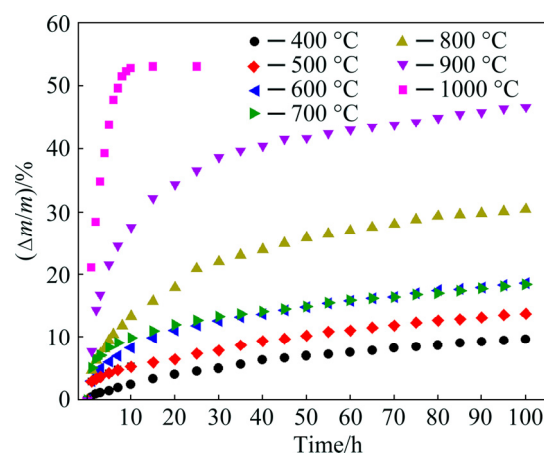


Fig. 3 Mass gain versus oxidation time plots of porous  $\text{Ti}_3\text{SiC}_2$  oxidized in air at 400–1000 °C

temperatures between 400 and 900 °C merely caused mass gains of less than 10%. The sample oxidized at 1000 °C obtained a total mass gain of 53% for only 10 h, and then the mass kept almost constant, suggesting that  $\text{Ti}_3\text{SiC}_2$  had been totally transformed into the corresponding oxides according to the stoichiometry of the overall oxidation reaction  $\text{Ti}_3\text{SiC}_2 + 6\text{O}_2 \rightarrow 3\text{TiO}_2 +$

$\text{SiO}_2+2\text{CO}_2$  [13,19]. It should be noted that the oxidation at 600 °C presented an accelerated trend in the late stage of oxidation and that after oxidation for 100 h the sample obtained a total mass gain (18.6%) larger than that (18.3%) at 700 °C. In general, the anomalous oxidation at ~600 °C was attributed to the cracks occurring during the oxidation process [25], which was shown in the SEM images of the section below.

### 3.2 XRD pattern and Raman spectrum analysis

As shown in Fig. 4(a), the samples after oxidation under the assigned conditions were inspected by XRD. The sample oxidized at 400 °C for 100 h mainly presented  $\text{Ti}_3\text{SiC}_2$  phase. However, it can be expected that a thin oxide scale must have been produced although the presence of oxides was not clearly demonstrated due to the poor sensitivity of XRD to the minor phases. After exposure at 600 °C for 50 h, the appeared oxides were predominantly identified as anatase and rutile  $\text{TiO}_2$ . With the increase of the oxidation temperature, the amount of rutile  $\text{TiO}_2$  increased while the  $\text{Ti}_3\text{SiC}_2$  amount decreased. The diffraction peaks for anatase  $\text{TiO}_2$  were hardly detected at 800 °C for 10 h. And a rapid oxidation occurred at 1000 °C. The intensities of  $\text{Ti}_3\text{SiC}_2$  peaks decreased dramatically after oxidation for only 1 h. When extending the duration to 10 h, the  $\text{Ti}_3\text{SiC}_2$  phase was no more detectable.

A more careful study of XRD measurements for the

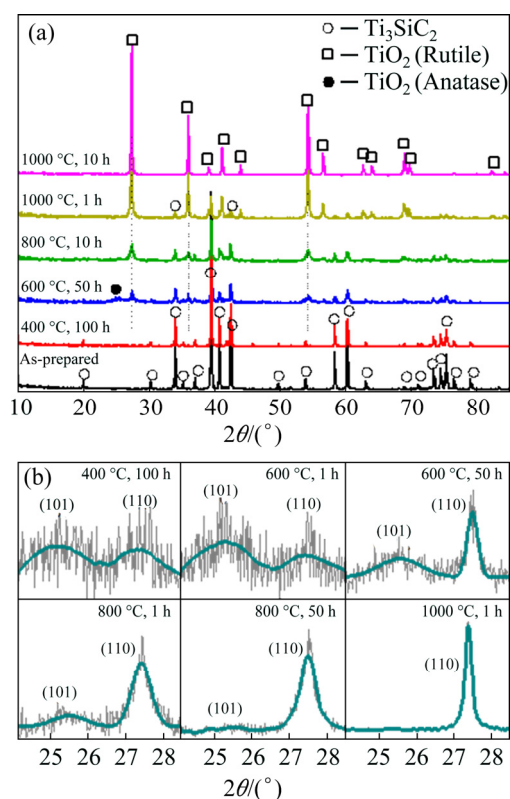


**Fig. 4** XRD patterns of samples oxidized at 400, 600, 800 and 1000 °C in air (a), and measurements of (101) peak of anatase  $\text{TiO}_2$  and (110) peak of rutile  $\text{TiO}_2$  in oxidized samples (b)

(101) diffraction peak of anatase and the (110) diffraction peak of rutile under various conditions was conducted in order to obtain the detail information of  $\text{TiO}_2$  modifications. The interferences from background noise were quite conspicuous for the diffraction peaks of  $\text{TiO}_2$  phases at 400 and 600 °C. Hence, the full curves were recreated by smoothing the original data with Savitzky–Golay method, as shown in Fig. 4(b). It is clearly seen that the XRD analysis result proved the presence of both anatase and rutile  $\text{TiO}_2$  at 400–800 °C. In general, anatase could be the primary crystal form of  $\text{TiO}_2$  at relatively low temperatures [26,27]. Thus, the rutile phase detected at 400–600 °C should be transformed from the metastable anatase phase. Note that the peak intensity of anatase phase was stronger than that of rutile phase at 400 °C for 100 h, while the case changed over at 600 °C for 50 h. This suggested that the anatase–rutile transformation was accelerated with the increase of the oxidation temperature. In addition, the diffraction peaks were broad at 400 °C (100 h) and 600 °C (1 h), indicating that the  $\text{TiO}_2$  products had a low crystallinity. The crystallite sizes of the  $\text{TiO}_2$  products were calculated to be ~5 μm according to Scherrer equation [26]. After oxidation at 600 °C for 50 h or at higher temperatures, the diffraction peaks became well resolved, indicating that the  $\text{TiO}_2$  crystals grew better and that the crystallite size got increased. In fact, the crystallization and grain growth were associated with heat emission [27–29]. Therefore, the exothermic peak III (~700 °C) in DSC curve might be potentially related to the crystallization of  $\text{TiO}_2$  products. For the sample oxidized at 800 °C for 1 h, the intensities of both anatase and rutile peaks increased rapidly compared with those at 600 °C. Note that the anatase  $\text{TiO}_2$  was initially the minor phase at this point. After oxidation at 800 °C for 50 h, almost no anatase peak could be detected. At 1000 °C, the oxide exhibited the XRD feature of rutile phase.

Regarding the low sensitivity of XRD to minor phases, Raman spectrum was thus employed for cooperatively analyzing the oxidation products, as shown in Fig. 5. At 400 °C, the bands of  $\text{TiO}_2$  products were quite weak. At 500 °C, the most intense Raman lines of anatase (at 151  $\text{cm}^{-1}$ ) and rutile (at 612  $\text{cm}^{-1}$ ) arose [30,31], showing an increase of  $\text{TiO}_2$  modifications in amount. At 600 °C, the Raman modes of anatase  $\text{TiO}_2$  at 151, 400, 515 and 639  $\text{cm}^{-1}$  were well resolved [31]. With the increase of the oxidation temperature, the intensities of Raman active bands (144, 240, 448, 612  $\text{cm}^{-1}$ ) for rutile  $\text{TiO}_2$  became stronger [31,32], and the peak widths were reduced. Notably, the strongest  $E_g$  mode at 151  $\text{cm}^{-1}$  (500–600 °C) assigned to nanocrystal anatase shifted to 144  $\text{cm}^{-1}$  (700–800 °C), which belonged to the single-crystal anatase [26]. These results proved the validity of the above inference about

exothermic peak III in Fig. 2(b). CAPWELL et al [32] have demonstrated the authenticity of  $143\text{ cm}^{-1}$  feature of rutile  $\text{TiO}_2$ , and have yielded a peak height intensity ratio of 0.065 ( $I_{143}/I_{612}$ ). Therefore, the  $144\text{ cm}^{-1}$  mode at raised temperatures should be a result of the superposition of  $E_g$  bands of anatase ( $144\text{ cm}^{-1}$ ) and rutile ( $143\text{ cm}^{-1}$ ). Obviously, the portion of intensity of  $144\text{ cm}^{-1}$  bands derived from rutile phase ought to increase with the rising of temperature. However, as the temperature rose, the  $144\text{ cm}^{-1}$  band got weakened, which indicated the reduction of anatase concentrations.

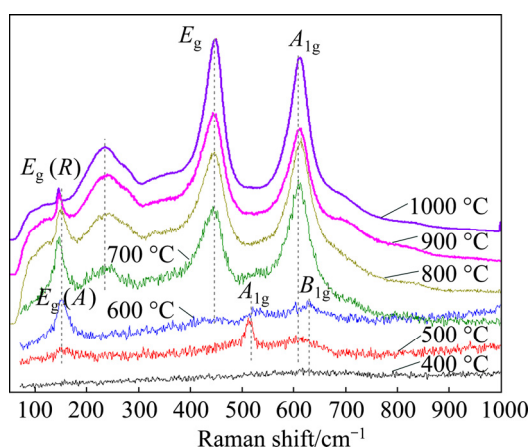


**Fig. 5** Raman spectra of porous  $\text{Ti}_3\text{SiC}_2$  samples after oxidation at 400–1000 °C for 10 h

According to the combined analyses of the XRD and Raman spectra, it can be seen that with the increase of the oxidation temperature, the relative content of anatase  $\text{TiO}_2$  firstly rose, and then decreased above 600 °C. The evolution of anatase amount presented the semblable trend as the exothermic behavior shown from peak I in Fig. 2(b), suggesting that the exothermic peak I at 400–700 °C might be related to anatase  $\text{TiO}_2$ , which subsequently transformed into rutile  $\text{TiO}_2$  [28,33]. The attenuation of the heat release above 600 °C in turn revealed that the diminution of anatase amount above 600 °C was due to the decrease of protogenetic anatase amount rather than the accelerated transformation rate at higher temperatures. In other words, at raised temperatures most Ti element has been directly oxidized into the high-temperature-stable rutile  $\text{TiO}_2$  [34].

### 3.3 Measurement of pore parameters

The changes of maximum pore size and permeability of porous  $\text{Ti}_3\text{SiC}_2$  during oxidation were measured to determine the pore-structure stability. As shown in Fig. 6(a), the maximum pore size of porous  $\text{Ti}_3\text{SiC}_2$  decreased overall with the duration of exposure. In the first 30 h of oxidation, the maximum pore sizes decreased from  $\sim 12.5$  to 10.2, 8.9, 9.7, and 9.6  $\mu\text{m}$  at 400, 600, 800, and 1000 °C, respectively. It is noted that the

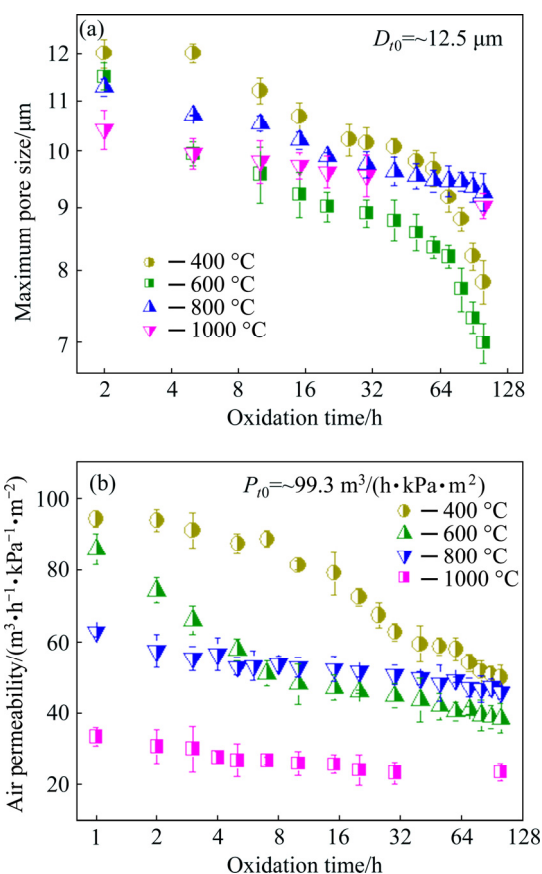


**Fig. 6** Maximum pore size (a) and gas permeability (b) as function of oxidation time for porous  $\text{Ti}_3\text{SiC}_2$  oxidized at 400, 600, 800 and 1000 °C, respectively

oxidation at 600 °C caused the largest decrement of maximum pore size in this stage. For the rest period of oxidation, the decrease of maximum pore size at 400 and 600 °C continued to maintain at a relatively high rate, while the decrease of that at 800–1000 °C was much more andante. The ultimate maximum pore sizes of samples oxidized at 400 and 600 °C reached 7.8 and 7.0  $\mu\text{m}$ , respectively, much lower than that of 9.3  $\mu\text{m}$  at 800 °C and that of 9.0  $\mu\text{m}$  at 1000 °C. The permeabilities of porous  $\text{Ti}_3\text{SiC}_2$  after oxidation at assigned temperatures showed similar variation tendency with pore size. As shown in Fig. 6(b), the decrement of permeability varied from 3.9 to 68.8  $\text{m}^3/(\text{h}\cdot\text{kPa}\cdot\text{m}^2)$  with increasing the oxidation temperature within 1 h. When extending the oxidation time to 7 h, abnormal decrease was also found in the samples tested at 400 and 600 °C. The ultimate permeabilities at 400 and 600 °C were very close to or even inferior to that at 800 °C. Above all, the oxidation temperature was still the primary factor affecting the pore parameters if excluding the influence of abnormal decrease.

### 3.4 Morphological observation

Figure 7 showed the SEM morphological structures

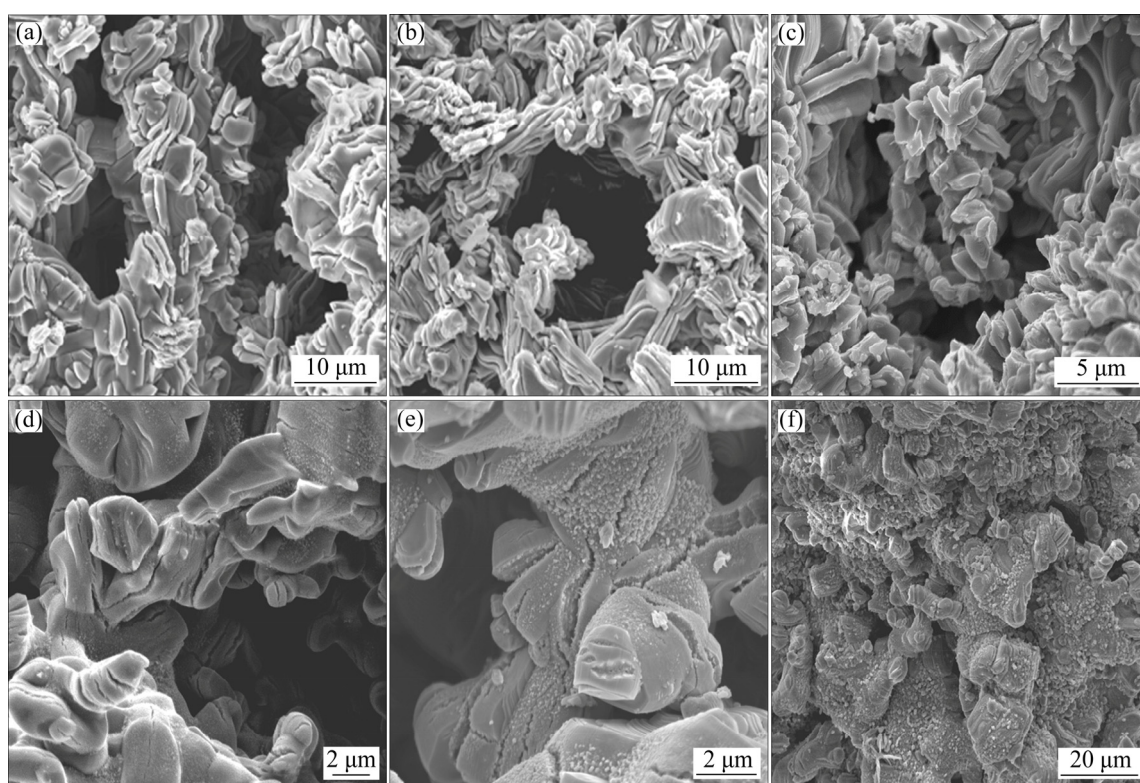


**Fig. 7** SEM images of porous  $\text{Ti}_3\text{SiC}_2$  oxidized in air at 400 °C for 50 h (a), 600 °C for 10 h (b), 600 °C for 50 h (c), 700 °C for 10 h (d), 800 °C for 10 h (e), and 1000 °C for 10 h (f), respectively

of the oxidized samples under different conditions. At 400 °C, the skeleton of porous  $\text{Ti}_3\text{SiC}_2$  mainly remained intact during the initial oxidation cycles (not shown). When extending the oxidation time to 50 h, a number of cracks were obviously observed on almost every grain in Fig. 7(a). The cracking condition of the specimen at 500 °C was similar to that at 400 °C. For the sample oxidized at 600 °C for 10 h, cracks were commonly observed, aligning along the laminations, as shown in Fig. 7(b). After exposure for 50 h, some of the grains were completely broken into several pieces (see Fig. 7(c)), which severely destroyed the original porous structures. For the samples oxidized at higher temperatures, the morphologies were quite different from those of the samples oxidized at 400–600 °C, as shown in Figs. 7(d–f). It is seen that the initial porous skeleton mainly kept integral although a few cracks were formed in the  $\text{Ti}_3\text{SiC}_2$  grains. As the oxidation temperature increased, the formation of the cracks got assuasive. Predicatively, the cracks could increase the specific surface area of porous  $\text{Ti}_3\text{SiC}_2$ . In order to confirm this, specific surface area measurements of the samples after oxidation at different temperatures for 10 h were carried out. The BET specific surface area of the sample oxidized at 600 °C reached a peak value of 0.48  $\text{m}^2/\text{g}$ , whereas those exposed to air at 400, 500, 700 and 800 °C were 0.13, 0.35, 0.33 and 0.31  $\text{m}^2/\text{g}$ , respectively. This result was consistent with the morphological properties

observed in Fig. 7. Moreover, it is found that the surfaces of the porous skeleton exposed at 800–1000 °C turned into rough appearance with some epitaxial oxide grains, as clearly shown in Fig. 7(e). Elemental analysis with EDS revealed that these oxides were  $\text{TiO}_2$  (not shown). At 1000 °C, a continuous surface layer composed of  $\text{TiO}_2$  crystals with a size of 500–800 nm covered the surface of porous skeleton (see Fig. 7(f)). In addition, a small amount of cracks were still observed on the surface of the porous skeleton.

## 4 Discussion

### 4.1 Evaluation of oxidation resistance

Figure 3 shows the mass gain curves of porous  $\text{Ti}_3\text{SiC}_2$  at different temperatures. It has been shown that the oxidation kinetics of porous  $\text{Ti}_3\text{SiC}_2$  samples was initially subparabolic, indicating that rapid oxidation took place in the initial period. With the establishment of protecting layer, the oxidation kinetics became linear. Long-term protection was generally associated with the diffusion-controlled process [35]. As the diffusion distance (scale thickness) increased with oxidation time, the rate of scale growth was slowed down. Unfortunately, the relatively high oxidation degree in the initial period set aside limited underlying unoxidized  $\text{Ti}_3\text{SiC}_2$  as the samples were just composed of micro-sized grains.

If using the oxidation kinetic trend as a gauge to characterize the severity of oxidation, the isothermal oxidation at ~600 °C was less deleterious than that in TG–DSC test. This discrepancy could be attributed to the anatase–rutile transformation. It is obvious that the oxidation rate depended primarily on the characteristics of the oxide products formed under the specific atmosphere and temperature. The detectable oxidation products of porous  $\text{Ti}_3\text{SiC}_2$  in the full temperature range of present work were  $\text{TiO}_2$  modifications, namely anatase and rutile. Anatase was the initial form of  $\text{TiO}_2$  products, which transformed into the rutile phase upon heating [27]. In the TG–DSC tests, samples were heated continually at a rate of 5.0 °C/min. The transformation of anatase was not sufficient until the temperature was raised above 600 °C [28]. The accumulated metastable anatase  $\text{TiO}_2$  gave little protection for the underlying substrate. For the samples experienced isothermal cyclic oxidation at 600 °C, however, the produced anatase was able to transform into rutile more sufficiently during the heating and cooling cycles. As a result, less anatase benefitted the mitigation of oxidation.

Nevertheless, neither anatase nor rutile is the identical oxide product used for protection. As far as we are aware, for long-term use above about 600 °C,  $\text{Cr}_2\text{O}_3$ ,  $\text{Al}_2\text{O}_3$  ( $\alpha$ ), and  $\text{SiO}_2$  are the principal protective oxides [35]. The metastable anatase was a kind of fast growing oxide which formed the less protective layers. Even for the high-temperature stabilized rutile phase, the self-diffusion rates of oxygen and Ti ions in the  $\text{TiO}_2$  crystal structure were inherently higher than those of  $\text{Al}_2\text{O}_3$  ( $\alpha$ ) and  $\text{SiO}_2$  because of the existence of oxygen interstitial and Ti vacancies [16]. In fact, it is generally accepted that the oxidation resistance of  $\text{Ti}_3\text{SiC}_2$  depended primarily on the amorphous  $\text{SiO}_2$  which has been widely identified in a number of reports [25,36,37]. Unfortunately, amorphous  $\text{SiO}_2$  was undetectable within the resolution of the X-ray diffractometer and Raman spectrum in the present experiments, but its existence could be predicted. The SEM images shown in Fig. 7 indicated that the generation of cracks severely ruptured the original  $\text{Ti}_3\text{SiC}_2$  grains, leading to the continuous exposure of fresh interface free of protection. Interestingly, no catastrophic oxidation mass gain was observed in the isothermal oxidation experiment at 600 °C, despite that the oxidation presented an accelerated trend. It is suggested that amorphous  $\text{SiO}_2$  could partially fill these cracks and prevent further oxidation. The role of amorphous  $\text{SiO}_2$  was also recognized in the oxidation of silicon nitride [38], silicon carbide [39], and Si-rich intermetallics [40].

#### 4.2 Evaluation of stability of pore structure

In general, the stability of pore structure during

high-temperature oxidation is determined by a complex interplay among characteristics of reaction products, such as microstructure, surface condition, and stress state. At 400–600 °C, although no visible growth of oxide scale could be observed in the SEM images shown in Figs. 7(a) and (b), a compact oxide scale on the surface of porous skeleton was believed to be produced through the direct reaction of  $\text{Ti}_3\text{SiC}_2$  with the dissolved or inward-diffused oxygen according to the oxidation kinetics. As shown in Fig. 6, the negative effect of the growth of oxide scale on the pore parameters at 400–600 °C in the initial hours was ignorable as compared with that at 800–1000 °C. The duration of oxidation at 400–600 °C led to the severe cracking of the  $\text{Ti}_3\text{SiC}_2$  grains, as shown in Figs. 7(a) and (b), which resulted in the significant decrease of pore size and permeability. The cripple of the mechanical integrity of porous skeleton not only reduced the equivalent aperture, but also increased the tortuosity of porous structure. As a result, the anomalous decrease in both pore size and permeability at lower temperatures took place. The cracks over 600 °C were limited. Therefore, the growth of oxide layer should be primarily responsible for the reasonable decrement in both maximum pore size and permeability. It is worth noting that the outward growth of oxide scales not only shrank the pore size, but also led to a decline in porosity and an increase of the pore-wall roughness (see Figs. 7(e) and (f)). These changes would dramatically deteriorate the connectivity of porous  $\text{Ti}_3\text{SiC}_2$ , thus increasing the resistance to gas flow. In this context, the decrement in permeability was generally exacerbated with the development of oxidation.

Previous studies showed that the oxidation of  $\text{M}_{n+1}\text{AX}_n$  materials at intermediate temperatures (below 700 °C) caused cracks which in turn led to the anomalous oxidation with higher kinetics [25,36,41]. Interestingly, in the present work, cracks were observed in the oxidized porous  $\text{Ti}_3\text{SiC}_2$  samples at 400–1000 °C (see Fig. 7). It is obvious that the occurrence of cracks was related to a kind of stress developed within the oxide layer, either growth stress or thermal stress. Table 1 shows the thermal expansion coefficients (TECs) of the main components in the oxidation system. The TECs of oxide products were higher than those of substrate at several comparable temperatures. At the cooling stage, the oxide layer bore tensile stress while the substrate suffered compressive stress, showing the possibility of initiation of cracks. However, this stress state was only able to cause the spallation of oxide layer, but incapable of rupturing the  $\text{Ti}_3\text{SiC}_2$  grains. Accordingly, it is suggested that thermal stress should not be mainly responsible for the abnormal cracks observed in the specific temperature range of 400–600 °C (but do not completely rule out this factor), while the cracks formed

**Table 1** Thermal expansion coefficients (TEC) of  $\text{Ti}_3\text{SiC}_2$ , anatase, rutile and  $\text{SiO}_2$ 

Component	Temperature/ $^{\circ}\text{C}$	$\alpha_a/(10^{-6} \text{ }^{\circ}\text{C}^{-1})$	$\alpha_c/(10^{-6} \text{ }^{\circ}\text{C}^{-1})$	$\alpha_v/(10^{-6} \text{ }^{\circ}\text{C}^{-1})$	Ref.
$\text{Ti}_3\text{SiC}_2$	698.2	7.87	7.23	26.3	[42]
	904.9	8.67	6.88	27.9	
	1233.5	8.08	9.49	30.5	
Anatase $\text{TiO}_2$	50	7.8	3.8	15.4	[43]
	690	20.4	9.5	39.4	
Rutile $\text{TiO}_2$	50	9.0	7.4	23.8	[43]
	690	13.4	9.1	31.6	
$\text{SiO}_2$	1200	12.3	–	–	[18]

$\alpha_a$  is the TEC of crystal in  $a$  axis;  $\alpha_c$  is the TEC of crystal in  $c$  axis;  $\alpha_v$  is the volumic TEC of crystal

under the cyclic oxidation conditions over  $600 \text{ }^{\circ}\text{C}$  could be ascribed to the effect of thermal stress. In fact, the abnormal cracks observed in the oxidation process of porous  $\text{Ti}_3\text{SiC}_2$  at  $400\text{--}600 \text{ }^{\circ}\text{C}$  have been similarly reported in the oxidation of  $\text{Ti}_3\text{AlC}_2$  [41] and  $\text{Ti}_2\text{AlC}$  [44] at intermediate temperatures. These works have employed the interpretation which was proposed in the oxidation of  $\text{TiC}$ , in which the cracks were associated with the stress resulting from the volume expansion due to the oxidation of  $\text{TiC}$  into anatase [27]. This stress was called bulk stress, which was an important form of growth stress [45]. Bulk stress can be calculated by the following equation: Pilling-Bedworth ratio  $\text{PBR} = V_{\text{ox}}/V_{\text{m}}$ , where  $V_{\text{ox}}$  and  $V_{\text{m}}$  are the volumes of the generated oxide and that of the lost metal for generating oxide, respectively.  $\text{PBR}=1$  is zero-bulk-stress status, while  $\text{PBR}>1$  indicates compressive stress in the oxide layer and tensile stress in the substrate. The formation of  $\text{TiO}_2$  and  $\text{SiO}_2$  from  $\text{Ti}_3\text{SiC}_2$  could cause volume expansion [36]. Accordingly, compressive stress was produced from the establishment of the surface oxide layer [27,36], which in turn gave rise to tensile stress in the substrate. It is worth noting that the density of anatase  $\text{TiO}_2$  ( $3.84 \text{ g/cm}^3$ ) is lower than that of rutile  $\text{TiO}_2$  ( $4.26 \text{ g/cm}^3$ ), which suggests that generation of anatase  $\text{TiO}_2$  at lower temperatures resulted in larger bulk stress. With the progress of oxidation, the bulk stress developing within the oxide layer would first crack the ledges of the lamellar structures which had flimsy cohesion [46,47], and eventually resulted in the destruction of porous frame.

## 5 Conclusions

1) High-purity porous  $\text{Ti}_3\text{SiC}_2$  with a porosity of 54.3% was fabricated and its oxidation behaviors were studied by investigating the oxidation kinetics, phase compositions, micro morphology, and pore-structure parameters during oxidation at temperatures from  $400$  to  $1000 \text{ }^{\circ}\text{C}$  in dry air.

2) At  $400\text{--}600 \text{ }^{\circ}\text{C}$ , the oxidation of  $\text{Ti}_3\text{SiC}_2$  produced a surface layer mainly composed of anatase  $\text{TiO}_2$  and amorphous  $\text{SiO}_2$ , which yielded great compressive stress that led to the cracking of  $\text{Ti}_3\text{SiC}_2$  grains. As a result, anomalous oxidation with higher kinetic and the abnormal decrease in pore size and permeability of porous  $\text{Ti}_3\text{SiC}_2$  were observed.

3) At  $700\text{--}1000 \text{ }^{\circ}\text{C}$ , the oxidation of porous  $\text{Ti}_3\text{SiC}_2$  was accelerated with the increase of temperature. The formation of cracks was limited due to the direct formation of rutile  $\text{TiO}_2$ . Since the oxidation layer did not provide the adequate protection for avoiding the rapid oxidation of porous  $\text{Ti}_3\text{SiC}_2$ , the outward growth of the oxide scales detrimentally affected the connectivity of the porous structure.

## References

- [1] BARSOUM M W. The  $\text{M}_{N+1}\text{AX}_N$  phases: A new class of solids: Thermodynamically stable nanolaminates [J]. Progress in Solid State Chemistry, 2000, 28: 201–281.
- [2] LIU Xin-li, JIANG Yao, ZHANG Hui-bin, HE Yue-hui. Corrosion behavior of porous  $\text{Ti}_3\text{SiC}_2$  in nitric acid and aqua regia [J]. Transactions of Nonferrous Metals Society of China, 2017, 27(3): 584–590.
- [3] GILBERT C, BLOYER D, BARSOUM M, EL-RAGHY T, TOMSIA A, RITCHIE R. Fatigue-crack growth and fracture properties of coarse and fine-grained  $\text{Ti}_3\text{SiC}_2$  [J]. Scripta Materialia, 2000, 42: 761–767.
- [4] RADOVIC M, BARSOUM M, EL-RAGHY T, SEIDENSTICKER J, WIEDERHORN S. Tensile properties of  $\text{Ti}_3\text{SiC}_2$  in the  $25\text{--}1300 \text{ }^{\circ}\text{C}$  temperature range [J]. Acta Materialia, 2000, 48: 453–459.
- [5] SHAN Di, YAN Guo, ZHOU Lian, LI Cheng-shan, LI Jin-shan, LIU Guo-qing, FENG Jian-qing. Synthesis of  $\text{Ti}_3\text{SiC}_2$  bulks by infiltration method [J]. Journal of Alloys and Compounds, 2011, 509: 3602–3605.
- [6] JACQUES S, DI-MURRO H, BERTHET M P, VINCENT H. Pulsed reactive chemical vapor deposition in the C–Ti–Si system from  $\text{H}_2/\text{TiCl}_4/\text{SiCl}_4$  [J]. Thin Solid Films, 2005, 478: 13–20.
- [7] WAN D T, ZHOU Y C, BAO Y W, YAN C K. In situ reaction synthesis and characterization of  $\text{Ti}_3\text{Si}(\text{Al})\text{C}_2/\text{SiC}$  composites [J]. Ceramics International, 2006, 32: 883–890.
- [8] LIU Xin-li, JIANG Yao, ZHANG Hui-bin, YU Lin-ping, KANG Jian-gang, HE Yue-hui. Porous  $\text{Ti}_3\text{SiC}_2$  fabricated by mixed

- elemental powders reactive synthesis [J]. *Journal of the European Ceramic Society*, 2015, 35: 1349–1353.
- [9] LIU Xin-li, ZHANG Hui-bin, JIANG Yao, HE Yue-hui. Characterization and application of porous  $\text{Ti}_3\text{SiC}_2$  ceramic prepared through reactive synthesis [J]. *Materials & Design*, 2015, 79: 94–98.
- [10] ABU M J, MOHAMED J J, AHMAD Z A. Synthesis of high purity titanium silicon carbide from elemental powders using arc melting method [J]. *Journal of Refractory Metals and Hard Materials*, 2014, 47: 86–92.
- [11] ZHOU C L, NGAI T W L, LU L, LI Y Y. Fabrication and characterization of pure porous  $\text{Ti}_3\text{SiC}_2$  with controlled porosity and pore features [J]. *Materials Letters*, 2014, 131: 280–283.
- [12] CHEN De-qiang, TIAN Xiang-jun, WANG Hua-ming, HUANG Zheng. Rapid synthesis of  $\text{TiC/Ti}_3\text{SiC}_2$  composites by laser melting [J]. *Journal of Refractory Metals and Hard Materials*, 2014, 47: 102–107.
- [13] SUN Z M, ZHOU Y C, LI M. High temperature oxidation behavior of  $\text{Ti}_3\text{SiC}_2$ -based material in air [J]. *Acta Materialia*, 2001, 49: 4347–4353.
- [14] RADHAKRISHNAN R, WILLIAMS J J, AKINC M. Synthesis and high-temperature stability of  $\text{Ti}_3\text{SiC}_2$  [J]. *Journal of Alloys and Compounds*, 1999, 285: 85–88.
- [15] TONG X, OKANO T, ISEKI T, YANO T. Synthesis and high temperature mechanical properties of  $\text{Ti}_3\text{SiC}_2/\text{SiC}$  composite [J]. *Journal of Materials Science*, 1995, 30: 3087–3090.
- [16] BARSOUM M, HO-DUC L, RADOVIC M, EL-RAGHY T. Long time oxidation study of  $\text{Ti}_3\text{SiC}_2$ ,  $\text{Ti}_3\text{SiC}_2/\text{SiC}$ , and  $\text{Ti}_3\text{SiC}_2/\text{TiC}$  composites in air [J]. *Journal of the Electrochemical Society*, 2003, 150: B166–B175.
- [17] YANG J, PAN L, GU W, GU X, SONG K, QIU T. Oxidation behavior and kinetics of in situ ( $\text{TiB}_2+\text{TiC}$ )/ $\text{Ti}_3\text{SiC}_2$  composites in air [J]. *Ceramics International*, 2012, 38: 159–168.
- [18] SARKAR D, PADHIARY A, CHO S J, CHU M C. Oxidation-induced strength behavior of  $\text{Ti}_3\text{SiC}_2$  [J]. *Journal of Materials Processing Technology*, 2009, 209: 641–646.
- [19] LI Shi-bo, CHENG Lai-fei, ZHANG Li-tong. Oxidation behavior of  $\text{Ti}_3\text{SiC}_2$  at high temperature in air [J]. *Materials Science and Engineering A*, 2003, 341: 112–120.
- [20] BARSOUM M W, EL-RAGHY T. Synthesis and characterization of a remarkable ceramic:  $\text{Ti}_3\text{SiC}_2$  [J]. *Journal of the American Ceramic Society*, 1996, 79: 1953–1956.
- [21] HE Yue-hui, JIANG Yao, XU Nan-ping, ZOU Jin, HUANG Bai-yun, LIU Jin-chuan. Fabrication of Ti–Al micro/nanometer-sized porous alloys through the Kirkendall effect [J]. *Advanced Materials*, 2007, 19: 2102–2106.
- [22] SUN Zi-qi, LIANG Ying, LI Mei-shuan, ZHOU Yan-chun. Preparation of reticulated MAX-phase support with morphology-controllable nanostructured ceria coating for gas exhaust catalyst devices [J]. *Journal of the American Ceramic Society*, 2010, 93: 2591–2597.
- [23] HERNÁNDEZ A, CALVO JI, PRÁDANOS P, TEJERINA F. Pore size distributions in microporous membranes: A critical analysis of the bubble point extended method [J]. *Journal of Membrane Science*, 1996, 112: 1–12.
- [24] ZHANG Z F, SUN Z M, HASHIMOTO H. Rapid synthesis of ternary carbide  $\text{Ti}_3\text{SiC}_2$  through pulse-discharge sintering technique from Ti/Si/TiC powders [J]. *Metallurgical and Materials Transactions A*, 2002, 33: 3321–3328.
- [25] ZHANG H B, ZHOU Y C, BAO Y W, WANG J Y. Oxidation behavior of bulk  $\text{Ti}_3\text{SiC}_2$  at intermediate temperatures in dry air [J]. *Journal of Materials Research*, 2006, 21: 402–408.
- [26] ZHANG W F, HE Y L, ZHANG M S, YIN Z, CHEN Q. Raman scattering study on anatase  $\text{TiO}_2$  nanocrystals [J]. *Journal of Physics D: Applied Physics*, 2000, 33: 912–916.
- [27] SHIMADA S, KOZEKI M. Oxidation of TiC at low temperatures [J]. *Journal of Materials Science*, 1992, 27: 1869–1875.
- [28] DABLER A, FELTZ A, JUNG J, LUDWIG W, KAISERSBERGER E. Characterization of rutile and anatase powders by thermal analysis [J]. *Journal of Thermal Analysis and Calorimetry*, 1988, 33: 803–809.
- [29] ZHANG Bao-long, CHEN Bai-shun, SHI Ke-yu, HE Shang-jin, LIU Xiao-dong, DU Zong-jie, YANG Ke-lian. Preparation and characterization of nanocrystal grain  $\text{TiO}_2$  porous microspheres [J]. *Applied Catalysis B: Environmental*, 2003, 40: 253–258.
- [30] PARKER J C, SIEGEL R W. Raman microprobe study of nanophase  $\text{TiO}_2$  and oxidation-induced spectral changes [J]. *Journal of Materials Research*, 1990, 5: 1246–1252.
- [31] CHANG H, HUANG P J. Thermo-Raman studies on anatase and rutile [J]. *Journal of Raman Spectroscopy*, 1998, 29: 97–102.
- [32] CAPWELL R J, SPAGNOLO F, DESESA M A. A rapid determination of low concentrations of anatase in rutile  $\text{TiO}_2$  pigments by Raman spectroscopy [J]. *Applied Spectroscopy*, 1972, 26: 537–539.
- [33] XU Wei, HU Wang-yu, LI Mei-heng, WEN Cui-e. Sol–gel derived hydroxyapatite/titaniabiocoatings on titanium substrate [J]. *Materials Letters*, 2006, 60: 1575–1578.
- [34] HE Gang, FANG Qi, ZHU Li-qiang, LIU Mao, ZHANG Li-de. The structure and thermal stability of  $\text{TiO}_2$  grown by the plasma oxidation of sputtered metallic Ti thin films [J]. *Chemical Physics Letters*, 2004, 395: 259–263.
- [35] BRADY M P, WRIGHT I G, GLEESON B. Alloy design strategies for promoting protective oxide-scale formation [J]. *JOM*, 2000, 52: 16–21.
- [36] RACAULT C, LANGLAIS F, NASLAIN R. Solid-state synthesis and characterization of the ternary phase  $\text{Ti}_3\text{SiC}_2$  [J]. *Journal of Materials Science*, 1994, 29: 3384–3392.
- [37] PANG W K, LOW I M, HANNA J V. Detection of amorphous silica in air-oxidized  $\text{Ti}_3\text{SiC}_2$  at 500–1000 °C by NMR and SIMS [J]. *Key Engineering Materials*, 2010, 434–435: 169–172.
- [38] CHU M C, CHO S J, PARK H M, YOON K J, RYU H. Crack healing in reaction-bonded silicon carbide [J]. *Materials Letters*, 2004, 58: 1313–1316.
- [39] TAKAHASHI K, KIM B S, CHU M C, SATO S, ANDO K. Crack healing behavior and static fatigue strength of  $\text{Si}_3\text{N}_4/\text{SiC}$  ceramics held under stress at temperature (800, 900, 1000 °C) [J]. *Journal of the European Ceramic Society*, 2003, 23: 1971–1978.
- [40] MCKAMEY C G, TORTORELLI P F, DEVAN J H, CARMICHAEL C A. A study of pest oxidation in polycrystalline  $\text{MoSi}_2$  [J]. *Journal of Material Research*, 1992, 7: 2747–2755.
- [41] WANG X H, ZHOU Y C. Oxidation behavior of  $\text{Ti}_3\text{AlC}_2$  powders in flowing air [J]. *Journal of Materials Chemistry*, 2002, 12: 2781–2785.
- [42] MANOUN B, SAXENA S K, LIERMANN H P, BARSOUM M W. Thermal expansion of polycrystalline  $\text{Ti}_3\text{SiC}_2$  in the 25–1400 °C temperature range [J]. *Journal of the American Ceramic Society*, 2005, 88: 3489–3491.
- [43] RAO K V K, NAIDU S V N, IYENGAR L. Thermal expansion of rutile and anatase [J]. *Journal of the American Ceramic Society*, 2006, 53: 124–126.
- [44] WANG X H, ZHOU Y C. Intermediate-temperature oxidation behavior of  $\text{Ti}_3\text{SiC}_2$  in air [J]. *Journal of Materials Research*, 2006, 21: 402–408.
- [45] QU H L, ZHOU L, WEI H R, ZHAO Y Q. Oxidation stratification of TiAl-based alloy [J]. *Chinese Journal of Nonferrous Metals*, 2001, 11(3): 398–403. (in Chinese)
- [46] FARLE A S, KWAKERNAK C, ZWAAG S V D, SLOOF W G. A conceptual study into the potential of  $\text{M}_{n+1}\text{AX}_n$ -phase ceramics for self-healing of crack damage [J]. *Journal of the European Ceramic Society*, 2015, 35: 37–45.
- [47] SONG G M, PEI Y T, SLOOF W G, LI S B, DE HOSSON J T M, VANDER ZWAAG S. Early stages of oxidation of  $\text{Ti}_3\text{AlC}_2$  ceramics [J]. *Materials Chemistry and Physics*, 2008, 112: 762–768.

## 反应合成 $\text{Ti}_3\text{SiC}_2$ 多孔材料的氧化行为

张惠斌<sup>1,2</sup>, 沈舒雨<sup>1</sup>, 刘新利<sup>2,3</sup>, 王重贺<sup>2</sup>, 江 垚<sup>2</sup>, 贺跃辉<sup>2</sup>

1. 浙江工业大学 材料科学与工程学院, 杭州 310014;
2. 中南大学 粉末冶金国家重点实验室, 长沙 410083;
3. 中南大学 材料科学与工程学院, 长沙 410083

**摘 要:** 采用反应合成方法制备孔隙度为 54.3% 的高纯  $\text{Ti}_3\text{SiC}_2$  多孔材料, 并研究其在 400~1000 °C 下空气中的氧化行为。采用热重-差热分析法、扫描电镜、X 射线衍射技术、能谱仪、拉曼光谱、BET 比表面分析法和孔结构测试等研究  $\text{Ti}_3\text{SiC}_2$  多孔材料在氧化前后的氧化动力学、物相组成、微观形貌以及孔结构参数演变。结果表明: 形成不同晶型  $\text{TiO}_2$  氧化产物是影响  $\text{Ti}_3\text{SiC}_2$  多孔材料抗氧化性及孔结构稳定性的主要因素。由于氧化产物体积应力以及热应力的存在, 因此, 在 400~1000 °C 试验过程中试样表面均出现开裂现象。其中, 在 400~600 °C 下形成的锐钛矿型  $\text{TiO}_2$  会导致  $\text{Ti}_3\text{SiC}_2$  晶粒出现严重开裂, 并引发快速氧化以及孔径和透气度的异常减小。600 °C 以上在氧化过程中主要形成金红石型  $\text{TiO}_2$ , 开裂现象得以缓解, 但是氧化膜的外延生长大幅降低了  $\text{Ti}_3\text{SiC}_2$  多孔材料孔隙的连通性。

**关键词:**  $\text{Ti}_3\text{SiC}_2$ ;  $\text{TiO}_2$ ; 多孔材料; 反应合成; 氧化

(Edited by Wei-ping CHEN)